

Quantum size effect of valence band plasmon energies in Si and SnO_x nanoparticles

H. Nienhaus,^{a)} V. Kravets, S. Koutouzov, C. Meier, and A. Lorke

Experimental Physics, University of Duisburg-Essen, Lotharstrasse 1, 47048 Duisburg, Germany

H. Wiggers

Combustion and Gas Dynamics, University of Duisburg-Essen, Lotharstrasse 1, 47048 Duisburg, Germany

M. K. Kennedy and F. E. Kruis

Department of Engineering Sciences, University of Duisburg-Essen, Bismarckstrasse 81, 47057 Duisburg, Germany

(Received 2 December 2005; accepted 1 March 2006; published 21 April 2006)

Spherical Si and SnO_x nanoparticles in the size range between 3 and 30 nm have been synthesized by microwave induced decomposition of silane and gas phase condensation, respectively. They are deposited on thin metal films and investigated by electron microscopy, Auger electron, and electron energy loss spectroscopy. An analysis of the surface composition and stoichiometry reveals that the Si particles are covered with a native oxide of less than 1 nm. The energy loss spectra show features corresponding to electronic excitations in the nanoparticles due to valence band plasmons, interband transitions, and core-level ionizations. The plasmon energies are found to increase with decreasing particle diameter d as $d^{-1.17}$ for Si and $d^{-0.83}$ for SnO_x. These energy shifts are related to the change of the dielectric band gap energy of the semiconductor due to quantum size effects. © 2006 American Vacuum Society. [DOI: 10.1116/1.2190658]

I. INTRODUCTION

Nanoparticle and cluster research has gained increasing attention since properties which are considered material parameters in the bulk become variables when the size of the particles is sufficiently reduced. This size effect is due to quantum confinement of elementary excitation within the nanometer-sized material. Examples which have been intensively investigated are excitons or phonons in low-dimensional semiconductor structures and nanoparticles.¹⁻³

Volume plasmons are long-wavelength, collective excitations of charge carriers.⁴ Within the nearly free electron model, the excitation energies are expected to be proportional to the square root of the charge carrier density. While this relationship is usually well fulfilled for dielectrics, it is violated in transition metals due to mixing of d - and s -electron states. Quantum size effects of plasmon energies have been widely studied for metal clusters and particles.^{3,5} Blue- as well as redshifts have been observed with decreasing size. They are attributed to either band structure effects, such as s - d mixing (e.g., in Ag) and band dispersion,⁵⁻⁷ or to reduced lifetimes of the plasmons due to surface scattering.³

Only a few studies exist on confinement effects of valence band plasmons in dielectrics⁸⁻¹⁵ although changes of the plasmon energy are of practical relevance for adjustable optical edge filters in the ultraviolet range. Due to the high excitation energies, electron energy loss spectroscopy (EELS) by inelastic electron scattering or photoemission has been used to investigate energy shifts. An increase of the plasmon energy with decreasing size or thickness has been reported for Si clusters,⁸ Si ultrathin films,¹¹ and porous Si⁹

as well as CdS quantum dots.¹³ The blueshift of plasmons in Si clusters was explained with the close relation between the plasmon and the electronic band gap energy. The latter is known to increase with smaller particle diameters d and, accordingly, the Si valence band plasmon energy has been reported to obey a $1/d^2$ dependence.⁸

The present study includes structural, chemical, and plasmonic investigations of Si and SnO_x nanoparticles, fabricated in the gas phase. A clear quantum size effect of the valence band plasmons is observed whereas interband transitions or core-level excitations remain unchanged. However, the measured blueshifts do not support the inverse square dependence.

II. EXPERIMENT

Agglomerates of monodisperse SnO_x nanoparticles, between 5 and 20 nm in diameter, were produced by gas condensation after evaporating SnO in a nitrogen atmosphere.¹⁶ Thermal treatments downstream follow for crystallization and sintering. The oxygen content x of the nanoparticles can be increased by adding oxygen gas to the aerosol stream and introducing an additional thermal oxidation step in a tube furnace. A narrow size distribution of the nanoparticles was confirmed by using a differential mobility analyzer (DMA).¹⁶ Finally, the nanoparticles were deposited on a 25 nm Pd film evaporated on a H-terminated Si(111) surface. The experimental setup for the synthesis of monodisperse SnO_x nanocrystal films is discussed in detail in Ref. 16. A scanning electron microscopy (SEM) image of deposited SnO_x nanoparticles with a diameter of 20 nm is shown in Fig. 1. It demonstrates the monodisperse character of the size distribution and the fractal shape of the agglomerates. The samples

^{a)}Electronic mail: nienhaus@uni-duisburg.de

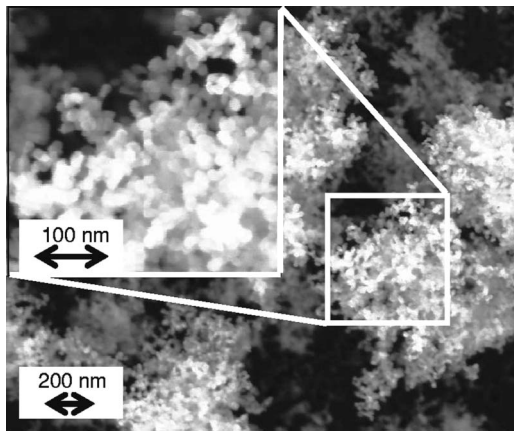


FIG. 1. Electron microscope image of monodisperse SnO_x nanoparticle agglomerates with a particle diameter of 20 nm.

were carried through air from the deposition to the analysis chamber where electron spectroscopy methods were performed.

Single crystalline silicon nanoparticles were synthesized by pyrolysis of silane in a low-pressure microwave reactor.¹⁷ The particles exhibit a log-normal size distribution.¹⁸ The average particle diameters are experimentally determined by the Brunauer-Emmett-Teller (BET) adsorption isotherm method¹⁹ and range from $d_{\text{BET}}=3.5$ to 27 nm. As demonstrated in the transmission electron microscopy (TEM) image in Fig. 2, the shape of the Si particles is almost spherical. Although in this sample $d_{\text{BET}}=4.8$ nm, predominantly larger particles can be identified in the transmission electron microscope image due to the low cross section of electron scattering for smaller particles. Throughout the article, the median d_M of the log-normal size distribution is used to quantify the Si nanoparticle sizes. It is related to d_{BET} by comparing the area of a particle with BET diameter with the second moment of the log-normal distribution,¹⁸ i.e.,

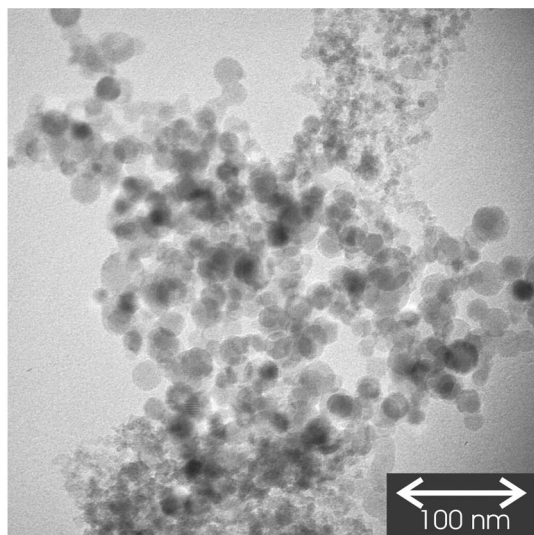


FIG. 2. Transmission electron microscope image of Si nanoparticles with an average diameter of $d_M=4.1$ nm.

$$d_M = \exp[\ln d_{\text{BET}} - \ln^2 \sigma], \quad (1)$$

where $\sigma=1.5$ is a typical standard deviation of the measured distribution of Si nanoparticle sizes.¹⁷ BET diameters of 3.5, 4.8, 11, 20, and 27 nm correspond to median values of 3.0, 4.1, 9.3, 17.0, and 22.9 nm.

After synthesis, macroscopic quantities of Si nanoparticle powder are recovered from the reactor. Since the particles are exposed to air, a natural oxide layer (~ 1 nm thick) is formed. For spectroscopic measurements, powder of agglomerated Si nanoparticles is sampled on a thin Au film by mechanical impregnation.²⁰

Auger electron spectroscopy (AES) is applied to determine the chemical composition of the nanoparticle surfaces. The spectra are recorded with 3 keV electron beam excitation in the first derivative mode using lock-in techniques. To investigate valence band plasmons and other electronic excitations of the nanoparticles, angle-integrated EELS was applied. The primary energy of the impinging electrons was adjusted to 100 eV and the spectra were recorded as the second derivative. As a consequence, the shape of the loss spectra are sensitive to the preparation of the nanoparticle film. The only significant experimental values are the peak positions of the loss features which appear at energies where the bulk loss function $\text{Im}\{-1/\epsilon(\omega)\}$ is maximum. If $\epsilon(\omega)$ is assumed to be a free electron dielectric function the energy loss features due to excitation of valence band plasmons are found at the plasmon energy $E_p = \hbar\omega_p = \hbar\{ne_0^2/m\epsilon_0\}^{0.5}$ (Ref. 4), where n is the valence electron density, m and e_0 are the electron mass and the elementary charge, respectively, and ϵ_0 denotes the permittivity of free space.

III. RESULTS AND DISCUSSION

A. Chemical composition (AES)

Figure 3 presents Auger spectra from SnO_x nanoparticles on Pd thin films as well as from sintered crystalline SnO_2 powder, taken as a reference. The most prominent features of the spectra can be attributed to C(*KLL*) at 270 eV kinetic energy, to Pd(*MNN*) at 333 eV, to the Sn(*MNN*) doublet at 421 and 429 eV, and to O(*KLL*) at 510 eV. The stoichiometry was determined from the intensity ratio between the O(*KLL*) and the low-energy Sn(*MNN*) line using the value of the bulk material as reference for SnO_2 . The two top spectra in Fig. 3 were recorded from $\text{SnO}_{1.5}$ particles of quite different size but do not exhibit significant differences. The Pd peak for the 5 nm particle film is larger due to lower particle coverage. The determined stoichiometry of 1.5 ± 0.1 is typical for SnO_x particles which are not further oxidized before deposition. It may be increased by additional heating of the samples in an oxygen atmosphere at 600 K for 1 h.²¹ The Auger spectrum of such oxidized nanoparticle films is displayed in Fig. 3 and labeled with $\text{SnO}_{1.8}$. It can be observed that the shape of the Sn Auger lines changes with oxidation as well. Inhomogeneous broadening due to variations in the chemical environments of the Sn atoms leads to a much less pronounced doublet.²¹

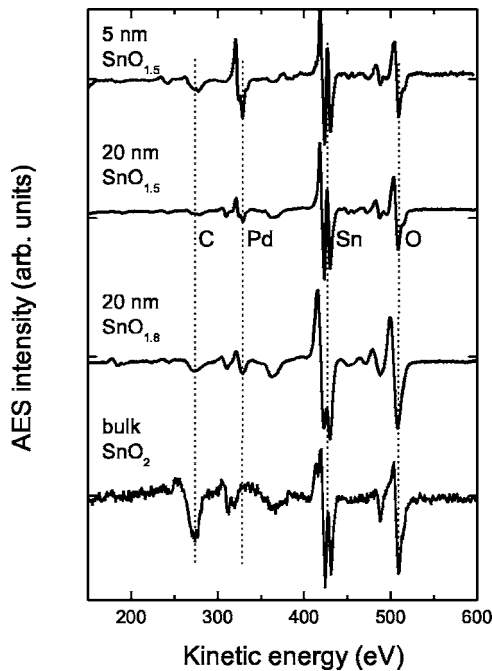


FIG. 3. Auger electron spectra of SnO_x nanoparticles of different sizes and stoichiometry deposited on Pd.

The chemical composition of Si nanoparticles deposited on Au films may be analyzed from the Auger electron spectra in Fig. 4. Besides the carbon and oxygen features, the Si(LVV) line at 91 eV kinetic energy dominates each spectrum. The varying shape of the low-energy side of the Si

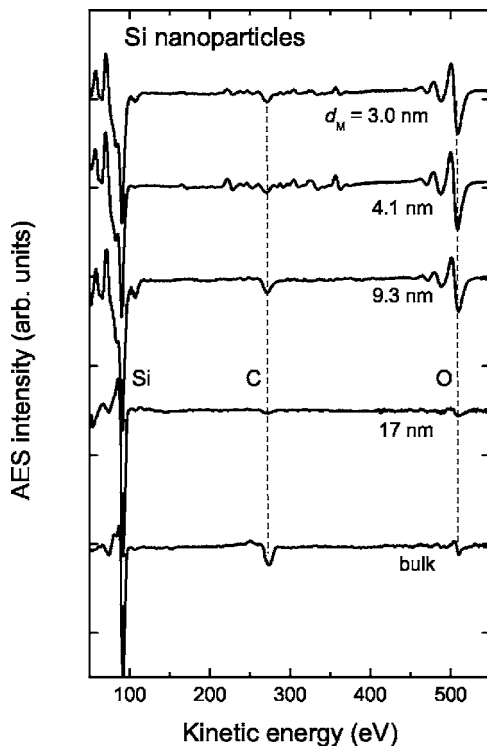


FIG. 4. Auger electron spectra of Si nanoparticles of different sizes deposited on Au.

feature is due to the Au Auger line at 69 eV which becomes more intense with decreasing nanoparticle coverage. The reference “bulk” spectrum was detected from a Si wafer which was first cleaned by the use of hydrofluoric acid and then oxidized by exposing it to air, similarly as the nanoparticle samples.

The structure at 91 eV originates from silicon atoms with no surrounding oxygen. It is still the dominating structure even in the spectra of the smallest particles. Therefore, the oxide layer around the nanoparticles has to be close to or thinner than the escape depth of the 91 eV Auger electrons which ranges between 0.5 and 1 nm. The oxygen intensity increases with decreasing particle size which may be explained by a simple geometric argument. The area of the Si core projected onto the substrate surface becomes smaller with decreasing particle diameter. Hence, the ratio between the O(KLL) and the Si(LVV) intensities will be larger than the bulk value. Assuming spherical particles with a uniform diameter d and an oxide layer thickness δ the ratio $(I_{\text{O}}/I_{\text{Si}})_{\text{ox}}$ added to the bulk value $(I_{\text{O}}/I_{\text{Si}})_{\text{b}}$ is expected to be proportional to the ratio of the SiO_2 shell and the Si core area projected onto the substrate surface, i.e.,

$$\begin{aligned} \frac{I_{\text{O}}}{I_{\text{Si}}} &= \left(\frac{I_{\text{O}}}{I_{\text{Si}}} \right)_{\text{b}} + C \frac{(d/2)^2 - (d/2 - \delta)^2}{(d/2 - \delta)^2} \\ &= \left(\frac{I_{\text{O}}}{I_{\text{Si}}} \right)_{\text{b}} + C \left(\frac{1}{(1 - 2\delta/d)^2} - 1 \right). \end{aligned} \quad (2)$$

In Eq. (2), it is assumed that the intensity of the Si feature at 91 eV originates from Si atoms of the core only. The equation allows a rough estimation for δ as long as the particle diameter is larger than the electron escape depth which is the case in the present study. To a first approximation, the constant C may be taken as the sensitivity ratio of the two Auger lines which may be extracted from literature data as $C \approx 0.2$ (Ref. 22). The bulk intensity ratio is measured as 0.1 in Fig. 4. Figure 5 shows the experimental intensity ratios of nanoparticles of various sizes as a function of the reciprocal of the median diameter. The shaded area is calculated according to Eq. (2) for an oxide thickness range between 0.5 and 1.2 nm and agrees with the experimental data within the error margins. The finding indicates that the SiO_2 layer around the Si nanoparticles is a native oxide with a typical thickness of less than 1 nm.

B. Electron energy loss spectra

Figure 6 presents EEL spectra recorded from SnO_x nanoparticles of different sizes and stoichiometries. Four prominent features are detected in each spectra. The low-energy structures at 6.5 and 12.5 eV are attributed to interband transitions (IT) in tin oxide. The loss feature at 27.3 eV is due to the Sn(4d) core-level ionization. The energies of these three energy losses do not depend on stoichiometry or the particle size. However, the feature between 17 and 20 eV shifts to lower energies with increasing particle size and may be identified as the valence band plasmon (PL) of SnO_x .^{23–25} The plasmon excitation energy does not change significantly after

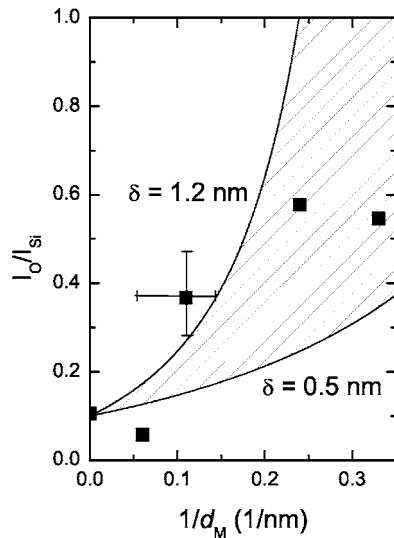


Fig. 5. Experimental ratio (data points) of oxygen and silicon Auger intensities as a function of the reciprocal of the median diameter. The shaded area represents the expected theoretical values according to Eq. (2) for oxide thicknesses between 0.5 and 1.2 nm.

annealing the sample in oxygen. No loss structures caused by electronic excitations in the Pd substrate layer are observed around 7.7 eV, indicating that the nanoparticle layer almost completely covers the metal substrate.

EEL spectra of Si nanoparticles with an oxide shell deposited on a thin Au film are displayed in Fig. 7. The spectrum at the bottom of the figure was recorded from a Si(111) wafer with native oxide. It shows the well-characterized loss features due to the SiO₂ volume plasmon at 22.5 eV, the Si volume plasmon at 16.0 eV, and the interface/surface plas-

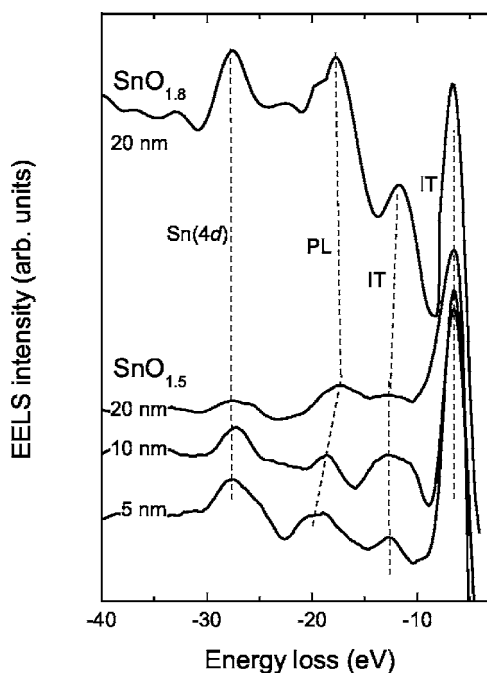


Fig. 6. EEL spectra from SnO_x nanoparticles. PL: plasmon loss, Sn(4d): core-level ionization, and IT: interband transition.

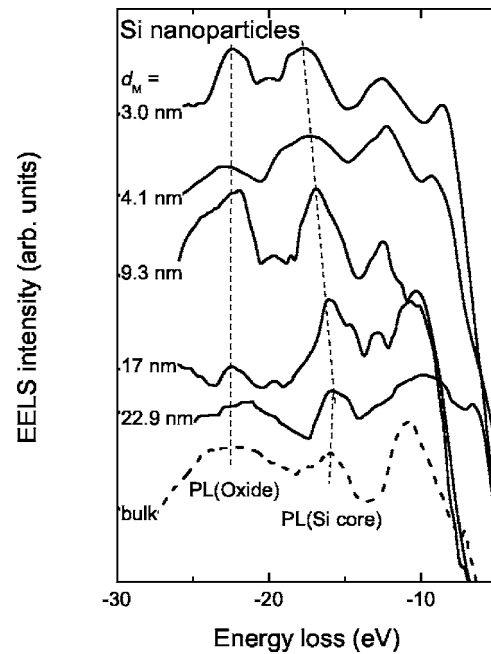


Fig. 7. EEL spectra from Si nanoparticles and the Si bulk sample.

mon at 10.7 eV.⁴ Such features are found in the spectra of the nanoparticles as well. However, other loss structures in the regime below 12 eV make an explicit identification difficult, since interband transitions and electronic excitations in the Au layer also occur in this energy range. Similar to the case of tin oxide, the valence electron plasmon exhibits a blueshift with decreasing size. The plasmon energy of the silicon oxide shell on the other hand is almost independent of the nanoparticle size. This finding agrees with the results from Auger spectroscopy that the oxide shell thickness is same for all particles.

The prominent blueshift of the Si and SnO_x valence plasmon energies is summarized in Fig. 8 where the excitation energies are plotted as a function of the diameter. It can be seen that the shift is an intrinsic property of the nanoparticle size and does not depend on the stoichiometry of the com-

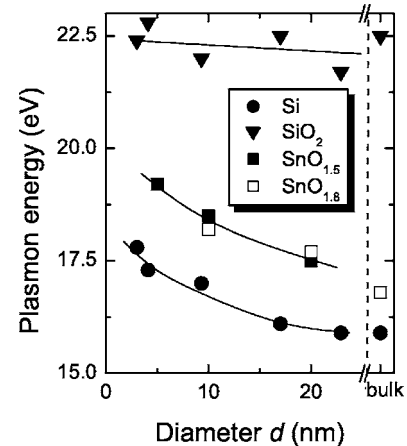


Fig. 8. Observed valence band plasmon energies as a function of the diameter of the particles.

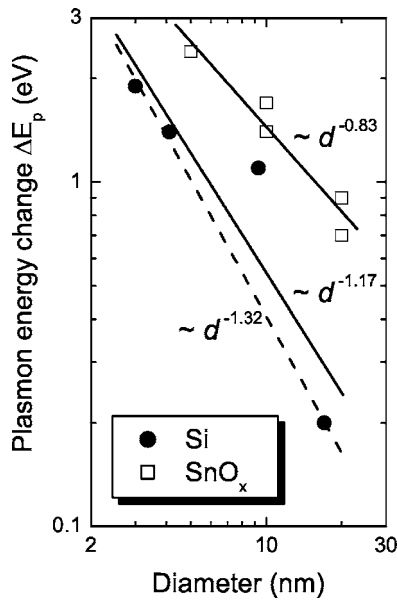


FIG. 9. Plasmon energy shift as a function of the diameter on a double logarithmic plot. The blueshifts obey a power law of the particle diameter.

pound material. Size effects of valence plasmon energies have been reported before, however, predominantly for metal particles.^{3,5} When the particle size is reduced, the lifetime of a plasmon decreases due to enhanced interface scattering. This leads to the well-characterized $1/d$ dependence of the plasmon loss linewidth and to a redshift of the plasmon energy with decreasing particle size in contrast to what is observed here.

Large blueshifts of valence band plasmon energies have been observed earlier with Si and CdS clusters of smaller diameters between 1 and 4 nm.^{8,13} The dispersion, i.e., the variation of the plasmon energy with wave vector k_{\parallel} cannot explain the extent of the energy shift. Considering the increased uncertainty of the wave vector with decreasing size and taking experimental plasmon dispersion parameters of Si, energy shifts are predicted in the 0.1 eV range for 3.5 nm clusters compared to the bulk value.⁸ The effect was explained by an enlarged gap energy due to quantum confinement of the electrons and a $1/d^2$ dependence of the plasmon energy shift was derived which is not observed in the present study.

To determine the exponent n of the $1/d^n$ dependence of the plasmon energy shift ΔE_p , Fig. 9 shows a double logarithmic plot of ΔE_p as a function of d . The data points are well described by power laws. The solid lines are linear fits and correspond to $n=0.83$ and 1.17 for tin oxide and silicon nanoparticles, respectively. The dashed line represents a fit with $n=1.32$ if the Si data point for $d=9.1$ nm which exhibits a very large experimental deviation is excluded. The two fits define the error margins of the determined exponents.

The findings may be explained by applying Penn's model of a semiconductor with an isotropic average band gap E_g which is related to the valence band plasmon energy in the long-wavelength limit by²⁶

$$\varepsilon_{\infty} = 1 + \left(\frac{E_p}{E_g} \right)^2, \quad (3)$$

where ε_{∞} is the static/electronic dielectric constant of the material. Pseudopotential calculations have shown that for Si nanoparticles with diameters above 2 nm the dielectric constant equals the bulk value.²⁷ Therefore, Eq. (3) suggests that the plasmon energy changes proportional to the band gap energy. For Si nanocrystals, the size dependence of the band gap energy has been experimentally studied with photoluminescence spectroscopy and the exponent was determined as $n=1.39$ (Ref. 28). This result agrees well with the value for Si nanoparticles from the present study. For tin oxide, size-dependent photoluminescence data are available for diameters between 1.5 and 4.3 nm which is smaller than the exciton Bohr radius.²⁹ No data exist for the size range of the present study and the exponent n cannot be determined.

IV. SUMMARY

Si and SnO_x nanoparticles of sizes between 3 and 27 nm are fabricated in the gas phase and deposited on Pd and Au thin films. Transmission electron microscopy confirms the spherical shape of the particles and demonstrates the narrow and broad size distribution for tin oxide and silicon nanoparticles, respectively. Auger electron spectroscopy shows that the Si particles are covered with a native oxide layer with thickness less than 1 nm. Valence band plasmons are detected with electron energy loss spectroscopy. Their energies shift to higher values with decreasing particle size. This finding is attributed to a quantum confinement model which leads to an increase of the band gap and, therefore, the plasmon energies. The applied model by Penn requires that the optical dielectric constant does not depend on the size which has to be investigated in further experiments.

ACKNOWLEDGMENT

The financial support by the Deutsche Forschungsgemeinschaft (DFG-SFB445) is gratefully acknowledged.

¹R. Schuster *et al.*, Phys. Status Solidi C **1**, 2028 (2004); C. Schulhauser *et al.*, *ibid.*, p. 2079.

²I. H. Campbell and P. M. Fauchet, Solid State Commun. **58**, 739 (1986).

³U. Kreibitz and M. Vollmer, *Optical Properties of Metal Clusters* (Springer, Berlin, 1995).

⁴H. Raether, *Excitations of Plasmons and Interband Transitions by Electrons* (Springer, Berlin, 1980).

⁵A. Liebsch, *Electronic Excitations at Metal Surfaces* (Plenum, New York, 1997).

⁶F. Ouyang, P. E. Batson, and M. Isaacson, Phys. Rev. B **46**, 15421 (1992).

⁷J. Tiggesbäumker, L. Köller, K. H. Meiwes-Broer, and A. Liebsch, Phys. Rev. A **48**, R1749 (1993).

⁸M. Mitome, Y. Yamazaki, H. Takagi, and T. Nakagiri, J. Appl. Phys. **72**, 812 (1992).

⁹S. Sato, S. Rath, S. Akiyama, S. Nozaki, and H. Morisaki, J. Appl. Phys. **86**, 1774 (1999).

¹⁰J. S. Yin and Z. L. Wang, Appl. Phys. Lett. **74**, 2629 (1999).

¹¹N. Dibiasi, G. Gabetta, A. Lumachi, M. Scagliotti, and F. Parmigiani, Appl. Phys. Lett. **67**, 2491 (1995).

¹²R. Massami Sasaki, F. Galembeck, and O. Teschke, Appl. Phys. Lett. **69**, 206 (1996).

¹³P. N. H. Nakashima, T. Tsuzuki, and A. W. S. Johnson, J. Appl. Phys. **85**,

- 1556 (1999).
- ¹⁴H. Hashimoto, S. Nishiuma, K. Takada, K. Nakamura, R. Ueno, and T. Den, *Jpn. J. Appl. Phys., Part 1* **38**, 4136 (1999).
- ¹⁵J. Wang, X. An, Q. Li, and R. F. Egerton, *Appl. Phys. Lett.* **86**, 201911 (2005).
- ¹⁶M. K. Kennedy, F. E. Kruis, H. Fissan, B. R. Metha, S. Stappert, and G. Dumpich, *J. Appl. Phys.* **93**, 551 (2003).
- ¹⁷J. Knipping, H. Wiggers, B. Rellinghaus, P. Roth, D. Konjhodzic, and C. Meier, *J. Nanosci. Nanotechnol.* **4**, 1039 (2004).
- ¹⁸C. G. Granqvist and R. A. Buhrman, *J. Appl. Phys.* **47**, 2200 (1976).
- ¹⁹S. Brunauer, P. H. Emmett, and E. Teller, *J. Am. Chem. Soc.* **60**, 309 (1938).
- ²⁰S. Koutousov, Diploma thesis, University of Duisburg-Essen, 2004.
- ²¹R. Ramamoorthy, M. K. Kennedy, H. Nienhaus, A. Lorke, F. E. Kruis, and H. Fissan, *Sens. Actuators B* **88**, 281 (2003).
- ²²S. Mroczkowski and D. Lichtman, *J. Vac. Sci. Technol. A* **3**, 1860 (1985).
- ²³G. B. Hoflund and G. R. Corallo, *Phys. Rev. B* **46**, 7110 (1992).
- ²⁴M. Bouslama, M. Ghamnia, C. Jardin, M. Bouderbala, and B. Gruzza, *Vacuum* **47**, 1353 (1996).
- ²⁵Y. Zhang and A. J. Slavin, *Phys. Rev. B* **49**, 2005 (1994).
- ²⁶D. R. Penn, *Phys. Rev.* **128**, 2093 (1962).
- ²⁷L.-W. Wang and A. Zunger, *Phys. Rev. Lett.* **73**, 1039 (1994).
- ²⁸G. Ledoux, O. Guillois, D. Porterat, C. Reynaud, F. Huisken, B. Kohn, and V. Paillard, *Phys. Rev. B* **62**, 15942 (2000).
- ²⁹E. J. H. Lee, C. Ribeiro, T. R. Girdali, E. Longo, E. R. Leite, and J. A. Varela, *Appl. Phys. Lett.* **84**, 1745 (2004).